

Swiss-cheese cosmologies with variable G and Λ from the renormalization group

Fotios K. Anagnostopoulos,^{1,*} Alfio Bonanno,^{2,3,†} Ayan Mitra^{4,5,6,‡} and Vasilios Zariikas^{7,5,§}

¹*Department of Informatics & Telecommunications, University of the Peloponnese, Karaiskaki 70, Tripoli 221 00, Greece*

²*INAF, Osservatorio Astrofisico di Catania, Via S. Sofia 78, 95123 Catania, Italy*

³*INFN, Sezione di Catania, Via S. Sofia 72, 95123 Catania, Italy*

⁴*The Inter-University Centre for Astronomy and Astrophysics (IUCAA), Post Bag 4, Ganeshkhind, Pune 411007, India*

⁵*Nazarbayev University, School of Engineering, Republic of Kazakhstan, 010000*

⁶*Kazakh-British Technical University, Tole bi 59, Almaty, Republic of Kazakhstan, 050000*

⁷*University of Thessaly, Department of Mathematics, 35100 Lamia, Greece*



(Received 10 January 2022; accepted 1 April 2022; published 27 April 2022)

A convincing explanation for the nature of the dark energy and dark matter is still missing. In recent works a RG-improved swiss-cheese cosmology with an evolving cosmological constant dependent on the Schücking radius has been proven to be a promising model to explain the observed cosmic acceleration. In this work we extend this model to consider the combined scaling of the Newton constant G and the cosmological constant Λ according to the IR-fixed point hypothesis. We shall show that our model easily generates the observed recent passage from deceleration to acceleration without need of extra energy scales, exotic fields or fine-tuning. In order to check the generality of the concept, two different scaling relations have been analyzed and we proved that both are in very good agreement with Λ CDM cosmology while one of them has no fine-tuning problem. We also show that our model satisfies the observational local constraints on \dot{G}/G .

DOI: [10.1103/PhysRevD.105.083532](https://doi.org/10.1103/PhysRevD.105.083532)

I. INTRODUCTION

Although the Λ CDM scenario reproduces rather well a large amount of observational data, it is important to stress that its two main ingredients, dark matter (DM) [1] and dark energy (DE) [2], do not have a direct physical explanation. In particular, the observed accelerated expansion of the Universe is caused by the DE component, a mechanism which introduces new difficulties in terms of fine-tuning or cosmic coincidences [3] for the presence of a significant vacuum energy (cosmological constant).

For this reason the possibility that the cosmological constant is dynamically generated as a low-energy quantum effect has been recently investigated by various authors [4,5]. In particular in [6] a cosmology with a time dependent cosmological constant and Newton constant whose dynamics arises from an underlying renormalization group flow near an infrared attractive fixed point has been proposed for the first time. Its phenomenological implications have been discussed in [7] and further developed in [8].

The IR-fixed point hypothesis originates from the asymptotically safe (AS) scenario for quantum gravity [9,10]. According to AS a consistent quantum theory of gravity can be realized nonperturbatively by defining the theory around a non-Gaussian fixed point for the dimensionless Newton's constant [11–19]. In fact this mechanism is not qualitatively different from what occurs in the nonlinear σ model in $d = 3$: here too, although the theory is not perturbatively renormalizable, a continuum limit at nonvanishing value of the coupling constant can be defined beyond perturbation theory [20,21].

Assuming that the relevant scale of energy or momentum scales with the distance as the coarse-graining, “resolution” scale of the renormalization group, the spatial or temporal evolution of the Newton's constant and cosmological constant is dictated by the renormalization group flow [19]. The possibility of explaining DM in spiral galaxies as an infrared effect of the running of G has been discussed in [22,23], while complete cosmological histories based on RG trajectories emanating from the UV fixed point up to the IR regime have been discussed in [24,25]. Nonsingular cosmological models have appeared in [26,27] and a mathematical formalism to couple the RG evolution to the Einstein equations have been discussed in [28,29].

*fotis-anagnostopoulos@hotmail.com

†alfio.bonanno@inaf.it

‡ayan.mitra@nu.edu.kz

§vzarikas@uth.gr

In [30] a further step in the direction of explaining the DE content in the Universe with a running cosmological constant has been proposed. The basic idea is to consider the contribution of an homogeneous distribution of antigravity sources associated with the matter content at galactic and cluster scale. A swiss-cheese cosmology represents an elegant mathematical framework to implement this idea which has been elaborated also in [31–33]. In this work we would like to extend the original RG-improved swiss-cheese model to include the running of the Newton’s constant according to the IR-fixed point mechanism. In this case, the scaling behavior of G and Λ is determined by the simple law

$$G_k \equiv G(k) \sim g_*/k^2, \quad \Lambda_k \equiv \Lambda(k) \sim \lambda_* k^2 \quad (1.1)$$

in the $k \rightarrow 0$ limit. This behavior could be the result of a “tree-level” renormalization induced by a nonzero positive cosmological constant in the IR, according to the singular behavior of the β functions in the IR [34–36]. The aim of this study is to further elaborate the IR-fixed point scaling within the swiss-cheese cosmology. In particular it will be shown that it is possible to consistently describe a phase of accelerated expansion of the universe without the introduction of a DE component.

The structure of this paper is the following: in Sec. II the mathematical structure of the swiss-cheese idea and the basic equations will be derived. In Sec. III the IR fixed point hypothesis and the RG evolution will be presented as a function of the Schücking radius and of the matter density. In Sec. IV the numerical results are discussed and finally, Sec. V is devoted to the conclusions.

II. SWISS-CHEESE COSMOLOGICAL MODEL

The original Einstein-Strauss model or otherwise called swiss-cheese model [37] describes many homogeneously distributed black holes smoothly matched within a cosmological metric. The key idea is to match a Schwarzschild spherical vacuole in a homogeneous isotropic cosmological spacetime. The analysis finally generates a dust Friedman-Robertson-Walker cosmology assuming many Schwarzschild black holes as the matter content.

It is also possible to show that respecting the Israel-Darmois matching conditions [38] a homogeneous and isotropic cosmological metric with a de Sitter-Schwarzschild-like metric can be successfully matched across a spherical 3-surface Σ which is at fixed coordinate radius of the cosmology metric frame (see also [39]). However, the radius of the surface in the black hole (BH) frame is time evolving. The matching requires the first fundamental form, intrinsic metric, and second fundamental form (extrinsic curvature), calculated in terms of the coordinates on Σ , to be equal (opposite for the second fundamental form) on both sides of the surface [40,41].

A homogeneous isotropic cosmological metric can be written in spherical coordinates as

$$ds^2 = -dt^2 + a^2(t)[r^2(d\theta^2 + \sin^2\theta d\phi^2) + (1 - \kappa r^2)^{-1}dr^2], \quad (2.1)$$

where $a(t)$ is the scale factor and $\kappa = 0, \pm 1$ is the spatial curvature constant.

The junction conditions [38] allow us to use different coordinate systems on both sides of the hypersurface. Thus, the cosmology exterior metric (2.1) can be joined smoothly to the following quantum-modified Schwarzschild metric [42]

$$ds^2 = -F(R)dT^2 + R^2(d\theta^2 + \sin^2\theta d\phi^2) + F(R)^{-1}dR^2, \quad (2.2)$$

where $F(R)$ is defined by

$$F(R) = 1 - \frac{2G_k M}{R} - \frac{\Lambda_k R^2}{3}. \quad (2.3)$$

Note that now the Newton constant and the cosmological constants are not constants but functions of one characteristic length scale $\sim 1/k$. Both will be functions of R as we shall explain later. The first fundamental form is the metric on Σ induced by the spacetime in which it is embedded. This may be written as

$$\gamma_{\alpha\beta} = g_{ij} \frac{\partial}{\partial u^\alpha} x^i \frac{\partial}{\partial u^\beta} x^j, \quad (2.4)$$

where $u^\alpha = (u^1 \equiv u, u^2 \equiv v, u^3 \equiv w)$ is the coordinate system on the hypersurface. Greek indices run over $1, \dots, 3$, while Latin indices over $1, \dots, 4$. The second fundamental form [38] is defined by

$$K_{\alpha\beta} = n_{i,j} \frac{\partial}{\partial u^\alpha} x^i \frac{\partial}{\partial u^\beta} x^j = (\Gamma^p_{ij} n_p - n_{i,j}) \frac{\partial}{\partial u^\alpha} x^i \frac{\partial}{\partial u^\beta} x^j, \quad (2.5)$$

where n_a is a unit normal to Σ and Γ^p_{ij} are the Christoffel symbols. We use subscripts F and S to denote quantities associated with the Friedman-Lemaître-Robertson-Walker (FLRW) and modified Schwarzschild metrics, respectively [41].

Let us consider a spherical hypersurface Σ given by the function $f_F(x^i_F) = r - r_\Sigma = 0$, where r_Σ is a constant. This hypersurface in the FLRW frame can be parametrized by $x^i_F = (t = u, \theta = v, \phi = w, r = r_\Sigma)$, while the parametrization in the BH frame is $x^i_S = (T = T_S(u), \theta = v, \phi = w, R = R_S(u))$. The fact that we model $R = R_S(u)$ implies that the hypersurface Σ may not remain in constant BH radial distance as the universe expands. This radial

distance is also called Schücking radius. The successful matching will prove that this choice of the matching surface was the appropriate thing to do for successful modeling of the junction. *From now on wherever in this section we write T and R we mean T_S and R_S , respectively.* The first Darmois condition $\gamma_{F\alpha\beta} = \gamma_{S\alpha\beta}$ gives

$$-1 = -F(R) \left(\frac{dT}{du} \right)^2 + F(R)^{-1} \left(\frac{dR}{du} \right)^2, \quad (2.6)$$

and

$$a^2 r_\Sigma^2 = R^2, \quad (2.7)$$

where, as we have explained, $R = R_S$. The last equation (2.7) is an important one and describes that the matching takes place in the hypersurface Σ where the BH radial distance is the time dependent Schücking radius R_S and the cosmological coordinate distance is the constant $r = r_\Sigma$.

The second Darmois condition requires to estimate the two second fundamental forms. First the normal vector, n_i , to the spherical hypersurface Σ has to be evaluated. If Σ is given by the function $f[x^\alpha(u^\alpha)] = 0$, then n_i can be calculated from

$$n_i = - \frac{f_{,i}}{\sqrt{|g^{ab} f_{,a} f_{,b}|}}, \quad (2.8)$$

where “ $,i$ ” denotes $\frac{\partial}{\partial x^i}$.

The (outward pointing) unit normal in the FLRW frame can be calculated from Eq. (2.8) and $f_F(x_F^i) = r - r_\Sigma = 0$. The result is

$$n_{Fi} = \left(0, 0, 0, - \left(\frac{a^2}{1 - kr_\Sigma^2} \right)^{1/2} \right). \quad (2.9)$$

Note, that the unit normal is spacelike, i.e., $n_F^i n_{Fi} = +1$. Since the equation of the matching surface $f_F(x_S^i)$ is unknown in the Schwarzschild frame the normal vector n_S^i cannot be calculated directly from Eq. (2.8). A condition for n_S^i can be derived from the partial differentiation of $x_S^i(u^\alpha)$ with respect to u^α which generates a tangential vector to the hypersurface Σ .

$$n_{Si} \frac{\partial x_S^i}{\partial u^\alpha} = 0, \quad (2.10)$$

From (2.10) one obtains $n_{S2} = n_{S3} = 0$ and

$$n_{S1} \frac{dT}{du} + n_{S4} \frac{dR}{du} = 0. \quad (2.11)$$

Furthermore, n_S^i must satisfy the identity

$$n_S^i n_{Si} \equiv n_F^i n_{Fi} = 1. \quad (2.12)$$

Then (2.12) gives

$$-(F(R))^{-1} n_{S1}^2 + F(R) n_{S4}^2 = 1. \quad (2.13)$$

Now using Eqs. (2.6), (2.13), and (2.11) it is possible to evaluate n_{Si} as a function of u^α :

$$n_{Si} = \left(\mp \frac{dR}{du}, 0, 0, \pm \frac{dT}{du} \right). \quad (2.14)$$

The second fundamental form can be easily calculated in the FLRW frame due to the simple form of n_{Fi} , Eq. (2.9). Thus from (2.5) we get

$$K_{F\alpha\beta} = \Gamma_{Fij}^4 n_{F4} \frac{\partial x_F^i}{\partial u^\alpha} \frac{\partial x_F^j}{\partial u^\beta} - n_{F4,j} \frac{\partial x_F^4}{\partial u^\alpha} \frac{\partial x_F^j}{\partial u^\beta}. \quad (2.15)$$

However, $\frac{\partial x_F^4}{\partial u^\alpha} = \frac{\partial r_\Sigma}{\partial u^\alpha} = 0$, and

$$\frac{\partial x_F^i}{\partial u^\alpha} \frac{\partial x_F^j}{\partial u^\beta} = \frac{\partial x_F^\mu}{\partial u^\alpha} \frac{\partial x_F^\nu}{\partial u^\beta} = \delta_\alpha^\mu \delta_\beta^\nu \quad (2.16)$$

so the second fundamental form becomes

$$\begin{aligned} K_{F\alpha\beta} &= n_{F4} \Gamma_{F\alpha\beta}^4, \\ &= -\frac{1}{2} |g_{F44}|^{1/2} g_F^{4i} (g_{Fai,\beta} + g_{F\beta i,\alpha} - g_{F\alpha\beta,i}), \\ &= \frac{1}{2} |g_{F44}|^{1/2} g_F^{44} g_{F\alpha\beta,4}, \end{aligned} \quad (2.17)$$

and finally

$$K_{F\alpha\beta} = \frac{1}{2} \left(\frac{a^2}{1 - kr^2} \right)^{-1/2} g_{F\alpha\beta,4}. \quad (2.18)$$

From Eq. (2.18) it is obvious that the only nonzero components of $K_{F\alpha\beta}$ are K_{F22} and K_{F33}

The estimation of the second fundamental form of Σ in the Schwarzschild frame is more complicated. First we have to calculate n_{Si} as a function of x_S^i . If we once more differentiate Eq. (2.10) with respect to u^α then it follows that

$$n_{Si,j} \frac{\partial x_S^i}{\partial u^\alpha} \frac{\partial x_S^j}{\partial u^\beta} = -n_{Si} \frac{\partial^2 x_S^i}{\partial u^\alpha \partial u^\beta}, \quad (2.19)$$

which, with the help of the definition equation (2.5), gives

$$K_{S\alpha\beta} = \Gamma_{Sij}^p n_{Sp} \frac{\partial x_S^i}{\partial u^\alpha} \frac{\partial x_S^j}{\partial u^\beta} + n_{Si} \frac{\partial^2 x_S^i}{\partial u^\alpha \partial u^\beta}. \quad (2.20)$$

Using Eq. (2.20), we find that $K_{S\alpha\beta} = 0$, $\forall \alpha \neq \beta$. This is true since the second derivative is zero for $\alpha \neq \beta$ and

the first term of Eq. (2.20) also is zero for $\alpha \neq \beta$ due to the specific Christoffel symbols.

The second Darms matching condition $K_{S\alpha\beta} = K_{F\alpha\beta}$ on Σ , provides the following differential equations

$$\begin{aligned} K_{S11} &\equiv \Gamma_{S11}^4 n_{S4} \left(\frac{dT}{du} \right)^2 + \Gamma_{S44}^4 n_{S4} \left(\frac{dR}{du} \right)^2 \\ &+ 2\Gamma_{S14}^1 n_{S1} \frac{dT}{du} \frac{dR}{du} + n_{S1} \frac{d^2T}{du^2} \\ &+ n_{S4} \frac{d^2R}{du^2} = 0 \equiv K_{F11}, \end{aligned} \quad (2.21)$$

since p can be either 1 or 4 for nonzero n_{Sp} and the only relevant nonzero Christoffel symbols $\Gamma_{Sij}^1, \Gamma_{Sij}^4$ are only $\Gamma_{S14}^1, \Gamma_{S41}^1$, and all Γ_{Sij}^4 . It is also

$$K_{S22} = K_{F22} \Leftrightarrow \Gamma_{S22}^4 n_{S4} = ar_{\Sigma} \sqrt{1 - \kappa r_{\Sigma}^2} \quad (2.22)$$

and

$$K_{S33} = K_{F33} \Leftrightarrow \Gamma_{S33}^4 n_{S4} = ar_{\Sigma} \sin^2 \theta \sqrt{1 - \kappa r_{\Sigma}^2}. \quad (2.23)$$

Now the relevant Christoffel symbols are $\Gamma_{S14}^1 = \frac{F'}{2F}, \Gamma_{S44}^4 = -\frac{F'}{2F}, \Gamma_{S11}^4 = \frac{1}{2}F(F'), \Gamma_{S22}^4 = -RF, \Gamma_{S33}^4 = -\sin^2 \theta RF$, where notation “'” is understood as derivative with respect to R .

Equations (2.22) and (2.23) being equivalent, we can use either of them and Eq. (2.7) to obtain

$$\frac{dT}{du} = \mp \frac{\sqrt{1 - \kappa r_{\Sigma}^2}}{1 - \frac{2G_k M}{R} - \frac{\Lambda_k R^2}{3}}. \quad (2.24)$$

It then follows from Eq. (2.6) that

$$\left(\frac{dR}{du} \right)^2 = \frac{2G_k M}{R} + \frac{\Lambda_k R^2}{3} - \kappa r_{\Sigma}^2. \quad (2.25)$$

Now differentiating Eqs. (2.24) and (2.25) with respect to u , we get the following expressions

$$\begin{aligned} \frac{d^2T}{du^2} &= \pm \sqrt{1 - \kappa r_{\Sigma}^2} \frac{d\left(+\frac{2G_k M}{R} + \frac{1}{3}\Lambda_k R^2\right)}{dR} \\ &\times \left(1 - \frac{2G_k M}{R} - \frac{1}{3}\Lambda_k R^2 \right)^{-2} \frac{dR}{du}. \end{aligned} \quad (2.26)$$

and

$$\frac{d^2R}{du^2} = \frac{1}{2} \frac{d\left(\frac{2G_k M}{R} + \frac{1}{3}\Lambda_k R^2\right)}{dR}. \quad (2.27)$$

With Eqs. (2.24)–(2.27), Eq. (2.21) is now identically satisfied. Thus, both the first and second fundamental forms are continuous on Σ .

Note that the cosmic evolution through the swiss cheese is determined by the cosmic evolution of the matching surface that is happening at spherical radius, in the black hole frame, R_S (and constant r_{Σ} for cosmic frame). This quantity enters the differential equations.

Finally, the matching requirements provide the following equations that are relevant for the cosmological evolution. *From this point and to the rest of the paper we use again separately the symbol R for the BH radial distance and the symbol R_S for the Schücking radius,*

$$R_S = ar_{\Sigma}, \quad (2.28)$$

$$\left(\frac{dR_S}{dt} \right)^2 = 1 - \kappa r_{\Sigma}^2 - \left(1 - \frac{2G_k(R_S)M}{R_S} - \frac{1}{3}\Lambda_k(R_S)R_S^2 \right), \quad (2.29)$$

$$2 \frac{d^2R_S}{dt^2} = \frac{d\left(\frac{2G_k(R)M}{R} + \frac{1}{3}\Lambda_k(R)R^2\right)}{dR} \Big|_{R_S}. \quad (2.30)$$

The matching radius r_{Σ} can be also understood as the boundary of the volume of the interior solid with energy density equal to the cosmic matter density ρ . Thus, the interior energy content should equal the mass M of the astrophysical object, i.e.,

$$r_{\Sigma} = \frac{1}{a_0} \left(\frac{2G_N M}{\Omega_{m0} H_0^2} \right)^{\frac{1}{3}}, \quad (2.31)$$

with density parameter $\Omega_m = \frac{8\pi G_N \rho}{3H^2} = \frac{2G_N M}{r_{\Sigma}^3 a^3 H^2}$ and a_0 set to be 1 for the rest of the analysis.

A rather important information in the context of the aforementioned approach is the exact physical element of our model, galaxies, clusters of galaxies or even super-clusters. In order to answer this, we should look at the physical interpretation of the Schücking radius, r_{Σ} , and its relation with measurable scales of the above astrophysical objects. For Milky Way ($M_{MW} \sim 4 \times 10^{11} M_{\odot}$) with typical values of cosmological parameters ($\Omega_{m0} \sim 0.3$, $H_0 \sim 67$ km/Mpc/s, [43]) using Eq. (2.31) we have $r_{\Sigma} \sim 1.4$ Mpc where the astrophysical radius is $R_{as} \sim 0.15$ Mpc. Similarly, for the Local Group $M_{LG} \sim (7-20) \cdot 10^{11}$ we find $r_{\Sigma} \sim 2.34$ Mpc and the astrophysical radius is $R_{as} \sim 1.53$ Mpc. Lastly, for the case of our local super-cluster, VIRGO ($M_{VSC} \sim 10^{15} M_{\odot}$) it is $R_{as} \sim 30.67$ Mpc and $r_{\Sigma} \sim 4$ Mpc. We observe that only in the scale of galaxy clusters it is r_{Σ}/R_{as} of order $\mathcal{O}(1)$, thus thereafter we will consider galaxy clusters as the elementary entities of the model.

Equations (2.28), (2.29), (2.30) for constants G_k and Λ_k reduce to the conventional FLRW expansion equations. However, although these equations generate the standard cosmological equations of the Λ CDM model, even in this simple case the interpretation is different since the Λ term appearing in the black hole metric [42] is like an average of all antigravity sources inside the Schücking radius of a galaxy or cluster of galaxies. These antigravity sources one can claim that may arise inside astrophysical black holes in the centers of which the presence of a quantum repulsive pressure could balance the attraction of gravity to avoid the not desired singularity, or they arise due to IR quantum corrections of a concrete quantum gravity theory. Furthermore, even for constant G_k and Λ_k the coincidence problem can be removed if the antigravity sources, due to the local effective positive cosmological constant, are related with the large scale structure that appears recently. In our analysis, we allow the running of G_k and Λ_k which is the most natural thing if there are IR quantum gravity corrections.

III. IR FIXED POINT AND COSMIC ACCELERATION

In this section the basic idea of the IR fixed point RG scaling will be introduced and the cosmic evolution of this model will be discussed.

A. The IR fixed point scaling

The presence of an IR instability in the RG flow for G and Λ is deeply rooted in the structure of the fluctuations determinant associated to the Einstein-Hilbert action

$$S_k = \frac{1}{16\pi G_k} \int dx^4 \sqrt{g} (-\mathcal{R} + 2\Lambda_k). \quad (3.1)$$

Let us consider a family of off shell spherically symmetric contributions labeled by the radius ϕ in order to distinguish the contributions from the two operators $\sqrt{g} \propto \phi^4$ and $\sqrt{g}\mathcal{R} \propto \phi^2$ to the Einstein-Hilbert flow [23]. It is possible to decompose the fluctuating metric $h_{\mu\nu}$ to the sphere into its irreducible pieces in terms of the corresponding spherical harmonics. In particular, in the transverse-traceless sector the operator $S_k^{(2)}$ is given by

$$-g^{\mu\nu} \nabla_\mu \nabla_\nu + 8\phi^{-2} + k^2 - 2\Lambda_k \quad (3.2)$$

up to a positive constant. If the spectrum of the covariant Laplacian $-g^{\mu\nu} \nabla_\mu \nabla_\nu u$ is non-negative, a singularity develops at a finite k in the case of a *positive* cosmological constant.

In a scalar field theory an identical mechanism is present when the Hessian of the action vanishes in the broken phase. In this case perturbation theory fails and the path integral is dominated by nonhomogeneous configurations [44] that produces a “tree-level” instability renormalization

already at level of the bare action [45]. In spite of the complexity of the vacuum structure, the approach based on functional flow equation is able to sum an infinite tower of (irrelevant UV) operator and it reproduces the correct flattening of the effective potential $U(\phi)$ in the broken phase [46]. In this case, below the coexistence line, the potential behaves as $U(\phi) \propto -k^2 \phi^2$ and approaches a flat bottom as $k \rightarrow 0$ [47].

In gravity the situation is more difficult because of the technical difficulties in solving the RG flow equation beyond the Einstein-Hilbert truncation in the $k \rightarrow 0$ limit [48–50]. Based on the analogy with the scalar theory one can imagine that a RG trajectory which realizes a tree-level renormalization exists [51]. In particular one can write that in the $k \rightarrow 0$ limit the dimensionless Newton constant and cosmological constant are attracted toward an IR fixed point (g_*, λ_*) according to the following trajectory

$$g(k) = g_* + h_1 k^{\theta_1}, \quad \lambda(k) = \lambda_* + h_2 k^{\theta_2}, \quad (3.3)$$

where $(\theta_1, \theta_2 \geq 0)$ are two unknown critical exponents. In terms of dimensionful quantities, we thus have

$$G(k)_{\text{IR}} = \frac{g_*}{k^2} + h_1 k^{\theta_1-2} \quad \Lambda(k)_{\text{IR}} = \lambda_* k^2 + h_2 k^{\theta_2+2}. \quad (3.4)$$

Here, k should be considered not as a momentum flowing into a loop, but as an inverse of a characteristic distance, of the physical system under consideration, over which the averaging of the field variables is performed. It can then be associated to the radial proper distance or the matter density.

For the rest of the paper in order to study the late cosmic evolution, we assume that the values of Newton constant and cosmological constant at the astrophysical scales will be those suggested in Eq. (3.4) i.e., $G_k = G(k)_{\text{IR}}$ and $\Lambda_k = \Lambda(k)_{\text{IR}}$.

In the first case we need to calculate the radial proper distance and in particular the Schücking proper radial distance, $D_p(R_S)$, which can be found from

$$D_p(R_S) = \int_{R_{\text{min}}}^{R_S} \frac{R}{\sqrt{F(R)}}, \quad (3.5)$$

where R_{min} is zero in our case or a very small value if AS provides a nonsingular black hole center, see [52]. Then, the derivative with respect to R is

$$D'_p(R_S) = \frac{1}{\sqrt{F(R_S)}} \quad (3.6)$$

Next, from matching Eqs. (2.28), (2.29), (2.30) we get

$$\left(\frac{dR_S}{dt} \right)^2 = 1 - \kappa r_\Sigma^2 - F(R_S), \quad (3.7)$$

which gives

$$r_\Sigma^2 \dot{a}^2 = 1 - \kappa r_\Sigma^2 - 1 + \frac{2G_k(R_S)M}{R_S} + \frac{1}{3}\Lambda_k(R_S)R_S^2 \quad (3.8)$$

and

$$\frac{\dot{a}^2}{a^2} = -\frac{\kappa}{a^2} + \frac{2G_k(R_S)M}{a^3 r_\Sigma^3} + \frac{1}{3}\Lambda(R_S). \quad (3.9)$$

B. Scaling using the cluster radial proper distance

Here the scaling we assume uses the proper distance

$$k = \frac{\xi}{D_p(z)}. \quad (3.10)$$

Using Eq. (3.9) we get

$$\frac{\dot{a}^2}{a^2} + k \frac{1}{a^2} = \chi + \psi, \quad (3.11)$$

where

$$\chi = 2 \left[\frac{g_*}{\xi^2} D_p^2 + h_1 \xi^{\theta_1 - 2} D_p^{2 - \theta_1} \right] M \frac{1}{r_\Sigma^3 a^3} \quad (3.12)$$

and

$$\psi = \frac{1}{3} [\lambda_* \xi^2 D_p^{-2} + h_2 \xi^{\theta_2 + 2} D_p^{-2 - \theta_2}]. \quad (3.13)$$

One useful quantity for evaluating the dark energy is the rate of change of the proper Schücking distance D_p . We have $\frac{dD_p}{dR} = \frac{dD_p}{dt} \frac{dt}{dR} = \frac{1}{\sqrt{F(R_S)}}$ and thus

$$\frac{dD_p}{dz} = \frac{-r_\Sigma}{(1+z)^2} \frac{1}{\sqrt{F}}, \quad (3.14)$$

where z is the redshift $z = -1 + \frac{1}{a}$ while the time derivative is

$$\dot{D}_p = \frac{r_\Sigma a H}{\sqrt{1 - \frac{2M}{ar_\Sigma} \left(\frac{g_*}{\xi^2} D_p^2 + h_1 \xi^{\theta_1 - 2} D_p^{2 - \theta_1} \right) - \frac{1}{3} (ar_\Sigma)^2 (\lambda_* \xi^2 D_p^{-2} + h_2 \xi^{2 + \theta_2} D_p^{-2 - \theta_2})}}. \quad (3.15)$$

The dark energy and dark matter part into the expansion equations is

$$H^2 + \frac{k}{a^2} = \frac{8\pi G_N \rho_{DM}}{3} + \frac{8\pi G_N \rho_{DE}}{3}, \quad (3.16)$$

where the dark energy and dark matter density are given by

$$\rho_{DE} = \frac{3}{8\pi G_N} \left[-\frac{2G_N M}{a^3 r_\Sigma^3} + \psi + \chi \right],$$

$$\rho_{DM} = \frac{3}{8\pi G_N} \frac{2G_N M}{a^3 r_\Sigma^3}. \quad (3.17)$$

The cosmological definition of the dust matter refers to a quality that evolves as $\sim a^{-3}$. In order to use the standard cosmological parameter Ω_{m0} so to easily compare our models with the concordance one, we extract from the ‘‘dark bulk’’ a portion that evolves as matter. Thus, the remaining one is correctly labeled as dark energy. Following the common parametrization the expansion can be written as

$$E^2 = \frac{H^2}{H_0^2} = \Omega_{DM} + \Omega_{DE} + \Omega_\kappa, \quad (3.18)$$

where

$$\Omega_{DM} = \frac{\rho_{DM}}{\rho_{cr}} \quad \text{and} \quad \Omega_{DE} = \frac{\rho_{DE}}{\rho_{cr}} \quad \text{and} \quad \Omega_\kappa = \frac{-\kappa}{a^2 H_0^2} \quad (3.19)$$

with $\rho_{cr} = \frac{3H_0^2}{8\pi G_N}$.

The cosmic acceleration, using Eq. (2.30), is then expressed as follows

$$2\frac{\ddot{a}}{a} + \frac{\dot{a}^2}{a^2} + \frac{\kappa}{a^2} = -8\pi G_N P, \quad (3.20)$$

where the total pressure is the sum of cosmic fluid pressure plus dark energy pressure $P = p + p_{DE}$. In the case of dust Universe $p = 0$, which is valid for small redshifts and since $H^2 + \kappa/a^2 = \chi + \psi$ we have

$$2\frac{\ddot{a}}{a} + \chi + \psi = -8\pi G_N p_{DE}. \quad (3.21)$$

Finally, the dark energy coefficient of equation of state is given by

$$w_{DE} = \frac{p_{DE}}{\rho_{DE}}. \quad (3.22)$$

In order to calculate the expansion of the Universe and the time evolution of the Ω_{DM} , Ω_{DE} , the equation of state parameter w_{DE} and the deceleration parameter $q = -\frac{\ddot{a}}{\dot{a}^2}$ we

must solve numerically ordinary differential equation (ODEs) for the scale factor and the proper distance. The relevant quantities as functions of the redshift are given below.

The derivative with respect to the redshift of the proper distance is

$$\frac{D_p}{dz} = -\frac{r_\Sigma}{(z+1)^2 \sqrt{-\frac{2M(z+1)\left(\frac{g_* D_p(z)^2}{\xi^2} + h_1\left(\frac{\xi}{D_p(z)}\right)^{\theta_1-2}\right)}{r_\Sigma} - \frac{r_\Sigma^2\left(h_2\left(\frac{\xi}{D_p(z)}\right)^{\theta_2+2} + \frac{\lambda_* \xi^2}{D_p(z)^2}\right)}{3(z+1)^2} + 1}}. \quad (3.23)$$

This is one of the differential equations we have to solve together with the expansion rate ODE for the scale factor Eq. (3.18)

$$q(z) = V^{-1} \left[6JMD_p(z)^5 \left(h_1 \left(\frac{\xi}{D_p(z)} \right)^{\theta_1} + g_* \right) + \frac{6\sqrt{3}Mr_\Sigma D_p(z)^4 \left(h_1(\theta_1 - 2) \left(\frac{\xi}{D_p(z)} \right)^{\theta_1} - 2g_* \right)}{z+1} \right. \\ \left. - \frac{2J\xi^4 r_\Sigma^3 D_p(z) \left(h_2 \left(\frac{\xi}{D_p(z)} \right)^{\theta_2} + \lambda_* \right)}{(z+1)^3} + \frac{\sqrt{3}\xi^4 r_\Sigma^4 \left(h_2(\theta_2 + 2) \left(\frac{\xi}{D_p(z)} \right)^{\theta_2} + 2\lambda_* \right)}{(z+1)^4} \right],$$

where

$$V = 2J \left(6MD_p(z)^5 \left(h_1 \left(\frac{\xi}{D_p(z)} \right)^{\theta_1} + g_* \right) + \frac{\xi^4 r_\Sigma^3 D_p(z) \left(h_2 \left(\frac{\xi}{D_p(z)} \right)^{\theta_2} + \lambda_* \right)}{(z+1)^3} \right) \quad (3.24)$$

and

$$J = \sqrt{-\frac{6M(z+1)D_p(z)^2 \left(h_1 \left(\frac{\xi}{D_p(z)} \right)^{\theta_1} + g_* \right)}{\xi^2 r_\Sigma} - \frac{\xi^2 r_\Sigma^2 \left(h_2 \left(\frac{\xi}{D_p(z)} \right)^{\theta_2} + \lambda_* \right)}{(z+1)^2 D_p(z)^2} + 3}, \quad (3.25)$$

where the today Schücking radius for a cluster of galaxies with mass M is

$$r_\Sigma = \sqrt{3} \frac{2G_N M}{H_0^2 \Omega_{DM0}} \quad (3.26)$$

the dark energy and dark matter part evolution is

$$\Omega_{DE}(z) = \frac{\Omega_{m0}(z+1)^3 \left(\frac{g_* D_p(z)^2}{\xi^2} + h_1 \left(\frac{\xi}{D_p(z)} \right)^{\theta_1-2} \right)}{G_N} \\ + \frac{h_2 \left(\frac{\xi}{D_p(z)} \right)^{\theta_2+2} + \frac{\lambda_* \xi^2}{D_p(z)^2}}{3H_0^2} - \Omega_{m0}(z+1)^3 \quad (3.27)$$

$$\Omega_{DM}(z) = \Omega_{m0}(z+1)^3. \quad (3.28)$$

The evolution of the dark energy coefficient is

$$w_{DE}(z) = \tilde{V}^{-1} r_\Sigma \left[\sqrt{3} r_\Sigma^3 \xi^4 \left(2\lambda_* + h_2(2 + \theta_2) \left(\frac{\xi}{D_p(z)} \right)^{\theta_2} \right) - 3\tilde{J} r_\Sigma^2 (1+z) \xi^4 \left[\lambda_* + h_2 \left(\frac{\xi}{D_p(z)} \right)^{\theta_2} \right] D_p(z) \right. \\ \left. - 6\sqrt{3}M(1+z)^3 \left(2g_* - h_1(-2 + \theta_1) \left(\frac{\xi}{D_p(z)} \right)^{\theta_1} \right) D_p(z)^4 \right],$$

where

$$\begin{aligned} \tilde{V} = 3\tilde{J}(1+z)^4 & \left[r_{\Sigma}^3 \xi^4 \left(\lambda_* + h_2 \left(\frac{\xi}{D_p(z)} \right)^{\theta_2} \right) D_p(z)/(1+z)^3 \right. \\ & \left. - 6G_N M \xi^2 D_p(z)^3 + 6M \left(g_* + h_1 \left(\frac{\xi}{D_p(z)} \right)^{\theta_1} \right) D_p(z)^5 \right] \end{aligned} \quad (3.29)$$

and

$$\tilde{J} = \left\{ 3 - \frac{r_{\Sigma}^2 \xi^2 [\lambda_* + h_2 (\frac{\xi}{D_p(z)})^{\theta_2}]}{(1+z)^2 D_p(z)^2} - \frac{6M(1+z)[g_* + h_1 (\frac{\xi}{D_p(z)})^{\theta_1}] D_p(z)^2}{r_{\Sigma} \xi^2} \right\}^{1/2}. \quad (3.30)$$

C. Scaling using the cluster density profile

Here, in this subsection we use another scaling,

$$k = \tilde{\xi} \rho_{cl}^{1/4}, \quad (3.31)$$

where the density of the cluster ρ_{cl} is

$$\rho_{cl} = \frac{\rho_c}{\left(\frac{\tilde{R}}{\alpha} \right)^{\beta} \left(\frac{\tilde{R}}{\alpha} + 1 \right)^{3-\beta}}, \quad (3.32)$$

where $\beta = 1/2$ and $\alpha = 226 \text{ kpc}$, and $\rho_c = 5.37 \times 10^6 M_{\odot} \text{ kpc}^{-3}$. The above density profile is of the type of the standard Navarro-Frenk-White profile. The parameter α , is the radius of the central cusp. This profile was used as a typical example of cluster profile [53].

To proceed further we set $\tilde{R} = D_p$ and using the matching equations we find that the derivative of the proper distance is given now by

$$D_p(z)/dz = - \frac{r_{\Sigma}}{(z+1)^2 \sqrt{-\frac{2M(z+1)A}{r_{\Sigma}} - \frac{r_{\Sigma}^2 B}{3(z+1)^2} + 1}}. \quad (3.33)$$

The Ω_{DM} remains the same but the Ω_{DE} is given by

$$\Omega_{\text{DE}} = \frac{2AM(z+1)^3}{H_0^2 r_{\Sigma}^3} + \frac{B}{3H_0^2} - \Omega_{m0}(z+1)^3, \quad (3.34)$$

where

$$\begin{aligned} A = & \left(\frac{g_*}{\tilde{\xi}^2 \sqrt{\frac{\rho_c}{\sqrt{\frac{D_p(z)}{\alpha} \left(\frac{D_p(z)}{\alpha} + 1 \right)^{5/2}}}}} \right. \\ & \left. + h_1 \left(\frac{\tilde{\xi} \sqrt{4} \frac{\rho_c}{\sqrt{\frac{D_p(z)}{\alpha} \left(\frac{D_p(z)}{\alpha} + 1 \right)^{5/2}}}}{\tilde{\xi}} \right)^{\theta_1-2} \right) \end{aligned} \quad (3.35)$$

and

$$\begin{aligned} B = & h_2 \left(\frac{\tilde{\xi} \sqrt{4} \frac{\rho_c}{\sqrt{\frac{D_p(z)}{\alpha} \left(\frac{D_p(z)}{\alpha} + 1 \right)^{5/2}}}}{\tilde{\xi}} \right)^{\theta_2+2} \\ & + \lambda_* \tilde{\xi}^2 \sqrt{\frac{\rho_c}{\sqrt{\frac{D_p(z)}{\alpha} \left(\frac{D_p(z)}{\alpha} + 1 \right)^{5/2}}}}. \end{aligned} \quad (3.36)$$

Unfortunately, expressions for $q(z)$ and a $w_{\text{DE}}(z)$ are quite long and thus are not presented here for economy of space.

IV. NUMERICAL RESULTS

In the following, we discuss the ability of our models to reproduce known observable quantities. Specifically, we check if there exist sets of free parameters that are able to reproduce the observed Hubble evolution within the acceptable range variation of the gravitational constant over time and the recent passage to cosmic acceleration. The existence of allowed range of parameters at the parameter space does not guarantee the fitting quality of our models, however the nonexistence implies the nonviability of our models. The full assessment of viability for our models ought to be performed using likelihood analysis and model selection methods on cosmological datasets, such as Supernovae Ia [54–57], baryonic acoustic oscillations [58] and direct measurements of the Hubble rate, in the same fashion with [33], will be presented in a forthcoming paper. This analysis is beyond the scope of the current work.

In what follows, we explicitly assume $\kappa = 0$, based upon observational results, i.e., cosmic microwave background (CMB) analysis [43]. In any case, even if the Universe is not exactly flat, the contribution of Ω_k to the expansion is negligible for recent redshifts like the ones that are relevant in our context.

We have decided to explore the free parameters space working with some simplified but reasonable assumptions. One should take into account that the evolution of G_k , must be smooth enough to comply with observational tests, i.e., solar system constraints [59,60] and astroseismology, [61]. A particular way to achieve this is to consider the first term in Eq. (3.4) to be subdominant to the second, thus allowing $G(k)$ to remain almost constant and have little dependence of k . In the same lines of reasoning, h_1 must be very close to

G_N . Therefore in our numerical assessments we set $h_1 = G_N$ and assume that θ_1 must be close to 2. On the other hand, as it has already been proven that a term proportional to k^2 , generates successful phenomenology [31–33] we also assume that θ_2 must be close to 0, and since both terms are practically proportional to k^2 , we can choose $\lambda_* \ll 1$. We further simplify our search for a viable cosmological model assuming

$$g_* \ll h_1 k_{\text{IR}}^{\theta_1}, \quad \lambda_* \ll h_2 k_{\text{IR}}^{\theta_2}, \quad (4.1)$$

where k_{IR} is the astrophysical scale. There are still many combinations of the remaining free parameters that can provide the correct phenomenology. A particularly simple way to find a subset of the parameter space that gives reasonable behavior from the phenomenological viewpoint is to ensure that

$$\chi(z \simeq 0) \sim \psi(z \simeq 0), \quad (4.2)$$

which happens if we use as initial condition for the differential equation that provides the evolution of the proper distance $D_p(z)$, the value from the requirement to have as $H(z=0)$ the current measured value of the Hubble rate. In general, the initial value that one gets for the proper distance in order to achieve the current value for $H(0)$ or Ω_{DE} to be the same as in the concordance model, could possibly give an unnatural value for the proper distance. In contrast, we obtain reasonable values that are of the same order and little bit larger than the Schücking radius of real astrophysical objects (clusters of galaxies) which is the correct thing. Furthermore, in order not to have new scales or fine-tuning we always give values close to order of one $O(1)$ for ξ and the dimensionless $\tilde{\gamma}$ which is related to h_2 from the definition $\tilde{\gamma} = h_2 G_N^{1-(\theta_2+2)/2}$.

Note, that in general the values of ξ and $\tilde{\xi}$ are different as Eq. (3.31) entails a very different scaling length. In the case of the first scaling that is associated with the proper distance and not the density, the natural length that appears in the differential equations, is the length scale at the matching surface. It is worth emphasizing at this point, that using this proper distance matching length scale [with ξ of $O(1)$], we get the correct amount of dark energy today after a recent passage from deceleration to acceleration while at the same time remarkably, this length scale is close to the natural astrophysical cluster length a fact that makes the

swiss-cheese model an acceptable approximation. The Schücking matching radius is close to the astrophysical cluster length. The fine-tuning problem is solved naturally in the first scaling but remains for the second scaling. It is of course not possible both scaling laws to solve the fine-tuning since the length scale that is derived from the proper distance at the matching, is very different from the length scale derived from the density at the matching surface. Note, that the values of the k and equivalently of the proper distance or of the density are evaluated in the matching surface and only these values enter the modified equations of motion. The study of the second scaling although does not solve the fine-tuning is useful since it provides both correct passage from deceleration to acceleration and correct dark energy equation of state coefficient behavior. These properties are not easily achievable or guaranteed that will occur. The very different length scale that is derived from the density at the matching surface, compared to the cluster length scale, is related with the large scale structure details. Another important thing to clarify is that the parameterization of the two scalings in AS context follows the same phenomenological reasoning. The quantity k should be increased as you go to a more energetic configuration of fields which means as you go closer to the center of the AS corrected de Sitter–Schwarzschild BH that models the cluster of galaxies.

In order to compare the Hubble rate in the context of AS models with the observations, we have to normalize accordingly the Hubble rate, i.e., to demand $H(0) = 100h$, where h is a dimensionless parameter and $h \in (0, 1)$. From this requirement, we can eliminate $\tilde{\gamma}$ from the Hubble rate demanding the matching to happen in $2r_\Sigma$, or we can have an initial condition for the $D_p(0)$ equal to a value close to r_Σ and fix $\tilde{\gamma}$. Thus, we can further manage to lower the number of free parameters for our models, which is beneficial from both conceptual and numerical viewpoints. In fact, we can also check if a particular instance of the model could describe the accelerated expansion of the Universe, while also satisfying the available observational constraints on \dot{G}/G . In Fig. 3 we illustrate three cosmological parameters for both scaling relations, with the total of 3 parameters, that are $(\xi, \theta_1, \theta_2)$ for the first scaling relation and $(\tilde{\xi}, \theta_1, \theta_2)$ for the second scaling relation. An indicative set of parameters that can give the desired phenomenology are listed in Table I.

TABLE I. Indicative points on the parameter space for each of the two scaling relations [Eqs. (3.10), (3.31)] that correspond to efficient phenomenology.

Scaling model	ξ or $\tilde{\xi}$	$\tilde{\gamma}$	θ_1	θ_2
Cluster radial proper distance $(\xi, \theta_1, \theta_2)$	3.0	3.0	2.001	0.06
\gg	1.0	0.1	2.005	0.05
Cluster density profile $(\tilde{\xi}, \theta_1, \theta_2)$	1×10^{-28}	10	2.001	0.06
\gg	1×10^{-28}	15	2.005	0.05

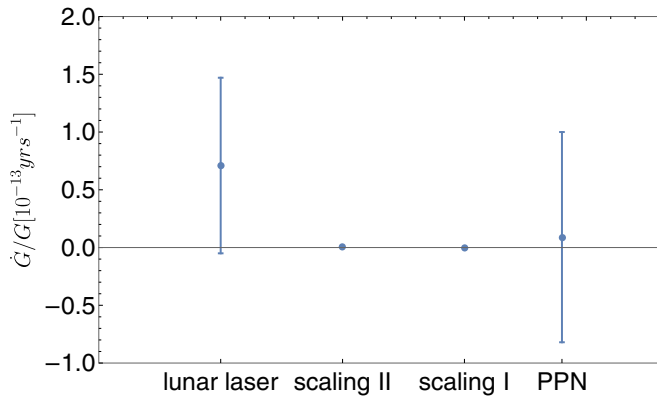


FIG. 1. Values of the normalized derivative of the Newton constant G around $z=0$, for both scaling relations labeled “scaling-I” which is the proper distance scaling and “scaling-II” the scaling using density. We include also the most recent observational values along with their error bars (1σ). These are (a) from [59] via calculating possible impact of varying G on planetary orbits (labeled “solar system orbits”) (b) from [60] using lunar laser ranging data (labeled “lunar laser”).

We also plot the most recent data compilation, that have obtained via the cosmic chronometers method, thus being approximately model independent, compiled at [62]. In addition we depict the Hubble rate of the concordance model (dashed black line) corresponding to the parameters set $\{\Omega_{m0}, h\} = \{0.3, 0.68\}$, to allow for qualitative comparison between the two models. The Hubble rate for each scaling relation is depicted with the solid line. Examination of Fig. 2 shows that both scenarios can give Hubble rate in close agreement with the observations.

Regarding the value of the normalized derivative of the coupling constant, \dot{G}/G today, we calculate $\dot{G}/G = -0.001 \times 10^{-13} \text{ yrs}^{-1}$ and $\dot{G}/G = 0.0083 \times 10^{-13} \text{ yrs}^{-1}$ for the first and the second scaling relations, respectively.

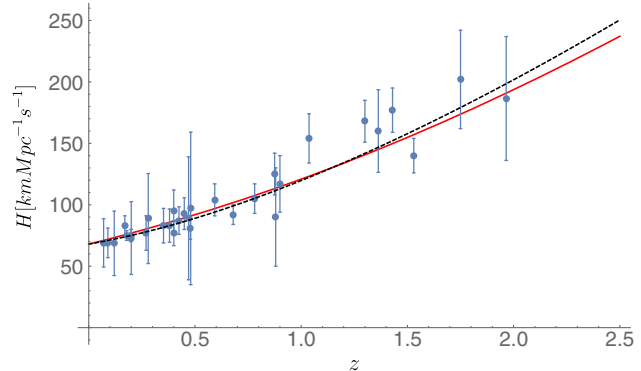
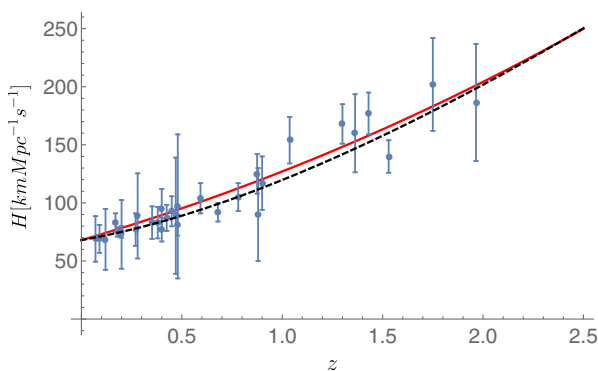


FIG. 2. Plot of the Hubble rate along with a subset of the observational dataset, containing only data points obtained via the cosmic chronometers method, compiled at [62]. To allow direct comparison, we depict the Hubble rate of the concordance model (dashed black line) corresponding to the parameters set $\{\Omega_{m0}, h\} = \{0.3, 0.68\}$. The Hubble rate for each scaling relation is depicted with the solid line. In all cases the initial condition for the solution of proper distance was set to be $2r_s$, for reasons explained in the text. Left: scaling using proper distance, for the parameter set $\{\Omega_{m0}, \xi, h, \theta_1, \theta_2\} = \{0.3, 0.68, 1, 2.001, 0.06\}$ Right: scaling using density, for the parameter set $\{\Omega_{m0}, h, \tilde{\xi}, \theta_1, \theta_2\} = \{0.3, 0.68, 10^{-28}, 2.005, 0.05\}$.

From Fig. 1, it is easy to observe that both models are within 1σ , that is in full agreement with the observational values from [59,60]. The same with the result from [61] which is one order of magnitude larger from the other two and is not depicted at Fig. 1. Figure 1 shows the comparison of these results with corresponding observations. As it is apparent from the latter figure, the evolution of G is within 1σ of the observed values, for both scaling relations.

As another viability test for our models, we use the transition redshift, defined via the requirement $q(z_{tr}) \equiv 0$. The latter corresponds to the moment of the transition between matter era and dark energy era in the cosmic history. In particular, using the plot of the deceleration parameter, q (second column of Fig. 3) for these particular instances of the two different scaling expressions, we find the transition redshift. For the case of scaling with proper distance, we have $z_{tr}^I \simeq 0.8$ which lies within $\sim 3\sigma$ of both [63] results, obtained via a model independent method. For the case of scaling using density, we obtain $z_{tr}^{II} \simeq 1$ which again is statistically compatible with [63] results. From the latter fact we deduce that both models seem to be viable.

V. CONCLUSIONS

In this work we have extended the swiss-cheese models presented in [30,33] to include an explicit running of G according to the IR fixed point hypothesis. The presented analysis generalizes the original Einstein-Strauss model by considering an interior vacuole spacetime described by a RG-improved Schwarzschild spacetime in the presence of a cosmological constant and Newton’s constant that depend either on the proper distance D_s , or on the matter density according to a RG trajectory for which both the dimensionless Newton constant and cosmological constant approach a fixed point at large distances.

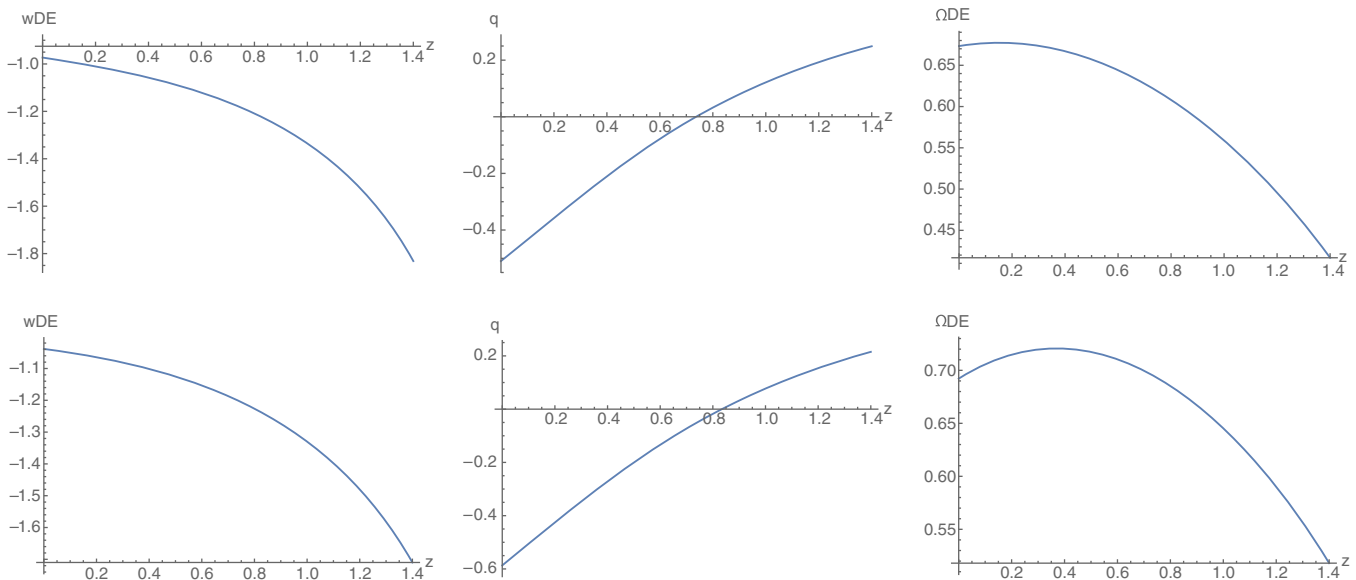


FIG. 3. Plots of some representative cosmological parameters. From left to right: equation of state parameter for the effective Dark Energy fluid, w_{DE} , deceleration parameter, q and normalized dark energy density, Ω_{DE} as a function of the redshift z , for the two different scaling relations (top and bottom panel), see text. The parameters used for these plots are (top panel) $\Omega_{m0} = 0.3, \xi = 1, \theta_1 = 2.001, \theta_2 = 0.04$, (bottom panel) $\Omega_{m0} = 0.3, \tilde{\xi} = 10^{-28}, \theta_1 = 2.005, \theta_2 = 0.06$.

The Darmois matching conditions determine the evolution of the FLRW spacetime outside the Schücking Radius. The RG trajectories emanating from the IR fixed point have been parametrized by two critical exponents θ_1 and θ_2 and by the scaling parameter ξ which relates the RG cutoff k with a characteristic distance scale. It turns out that the present phase of accelerated expansion is the result of the cumulative antigravity sources contribution within the Schücking radius. In particular no fine-tuning emerges at late times. Our formalism allows us also to take into account of the constraints on \dot{G}/G . Albeit the parameter space is large and a full numerical analysis is beyond the scope of the present work, it was possible to find many set parameters which reproduce the current Λ CDM standard model. The results are very encouraging, as for both scaling

expressions we do obtain reasonable behavior for the cosmological quantities $H(z)$, q , w_{DE} , and Ω_{DE} .

Interesting enough for the interesting cases both θ_1 and θ_2 can be taken as positive and this is consistent with the idea that the IR fixed point must be attractive in the $k \rightarrow 0$ limit. It would therefore be interesting to further test this cosmological model against the current observational data in the spirit of [64,65].

ACKNOWLEDGMENTS

The authors acknowledge the support of the Faculty Development Competitive Research Grant Program (FDCRGP) Grant No. 110119FD4534. We are grateful to Alessia Platania for important remarks and comments on the manuscript.

-
- [1] V.C. Rubin and W.K. Ford, Jr., *Astrophys. J.* **159**, 379 (1970).
 - [2] D. N. Spergel, R. Bean, O. Doré, M. R. Nolta, C. L. Bennett, J. Dunkley, G. Hinshaw, N. Jarosik, E. Komatsu, L. Page *et al.*, *Astrophys. J. Suppl. Ser.* **170**, 377 (2007).
 - [3] N. Straumann, *Eur. J. Phys.* **20**, 419 (1999).
 - [4] Q. Wang, Z. Zhu, and W.G. Unruh, *Phys. Rev. D* **95**, 103504 (2017).
 - [5] S. Carlip, *Phys. Rev. Lett.* **123**, 131302 (2019).
 - [6] A. Bonanno and M. Reuter, *Phys. Lett. B* **527**, 9 (2002).
 - [7] E. Bentivegna, A. Bonanno, and M. Reuter, *J. Cosmol. Astropart. Phys.* **01** (2004) 001.
 - [8] A. Bonanno and S. Carloni, *New J. Phys.* **14**, 025008 (2012).
 - [9] S. Weinberg, in *General Relativity: An Einstein Centenary Survey*, edited by S. W. Hawking and W. Israel (Cambridge University Press, Cambridge, 2010), pp. 790–831.
 - [10] M. Reuter, *Phys. Rev. D* **57**, 971 (1998).
 - [11] D.F. Litim, *Phil. Trans. R. Soc. A* **369**, 2759 (2011).
 - [12] S. Nagy, *Ann. Phys. (Amsterdam)* **350**, 310 (2014).

- [13] A. Bonanno and F. Saueressig, *C.R. Phys.* **18**, 254 (2017).
- [14] R. Percacci, *An Introduction to Covariant Quantum Gravity and Asymptotic Safety, 100 Years of General Relativity* (World Scientific, Singapore, 2017), Vol. 3.
- [15] A. Eichhorn, *Front. Astron. Space Sci.* **5**, 47 (2019).
- [16] A. D. Pereira, [arXiv:1904.07042](https://arxiv.org/abs/1904.07042).
- [17] M. Reuter and F. Saueressig, *Quantum Gravity and the Functional Renormalization Group: The Road towards Asymptotic Safety* (Cambridge University Press, Cambridge, England, 2019).
- [18] M. Reichert, *Proc. Sci.*, 384 (2020) 005.
- [19] A. Platania, *Front. Phys.* **8**, 188 (2020).
- [20] A. M. Polyakov, in *Les Houches Summer School on Gravitation and Quantizations, Session 57* (1993), pp. 0783–804, [arXiv:hep-th/9304146](https://arxiv.org/abs/hep-th/9304146).
- [21] A. Codello and R. Percacci, *Phys. Lett. B* **672**, 280 (2009).
- [22] M. Reuter and H. Weyer, *Phys. Rev. D* **70**, 124028 (2004).
- [23] M. Reuter and H. Weyer, *J. Cosmol. Astropart. Phys.* **12** (2004) 001.
- [24] M. Reuter and F. Saueressig, *J. Cosmol. Astropart. Phys.* **09** (2005) 012.
- [25] A. Bonanno and M. Reuter, *J. Cosmol. Astropart. Phys.* **08** (2007) 024.
- [26] G. Kofinas and V. Zariikas, *Phys. Rev. D* **94**, 103514 (2016).
- [27] A. Bonanno, S. J. G. Gionti, and A. Platania, *Classical Quantum Gravity* **35**, 065004 (2018).
- [28] M. Reuter and H. Weyer, *Phys. Rev. D* **69**, 104022 (2004).
- [29] A. Bonanno, G. Kofinas, and V. Zariikas, *Phys. Rev. D* **103**, 104025 (2021).
- [30] G. Kofinas and V. Zariikas, *Phys. Rev. D* **97**, 123542 (2018).
- [31] A. Mitra, V. Zariikas, A. Bonanno, M. Good, and E. Güdekli, *Universe* **7**, 263 (2021).
- [32] F. K. Anagnostopoulos, G. Kofinas, and V. Zariikas, *Int. J. Mod. Phys. D* **28**, 1944013 (2019).
- [33] F. K. Anagnostopoulos, S. Basilakos, G. Kofinas, and V. Zariikas, *J. Cosmol. Astropart. Phys.* **02** (2019) 053.
- [34] S. Nagy, J. Krizsan, and K. Sailer, *J. High Energy Phys.* **07** (2012) 102.
- [35] N. Christiansen, D. F. Litim, J. M. Pawłowski, and A. Rodigast, *Phys. Lett. B* **728**, 114 (2014).
- [36] J. Biemans, A. Platania, and F. Saueressig, *Phys. Rev. D* **95**, 086013 (2017).
- [37] A. Einstein and E. G. Straus, *Ann. Math.*, **47** 731 (1946).
- [38] L. P. Eisenhart, *Riemannian Geometry* (Princeton University Press, Princeton, NJ, 2016).
- [39] R. Balbinot, R. Bergamini, and A. Comastri, *Phys. Rev. D* **38**, 2415 (1988).
- [40] G. Darrois, *Les équations de la Gravitation Einsteinienne* (Gauthier-Villars Paris, Paris, 1927).
- [41] C. C. Dyer and C. Oliwa, [arXiv:astro-ph/0004090](https://arxiv.org/abs/astro-ph/0004090).
- [42] B. Koch and F. Saueressig, *Int. J. Mod. Phys. A* **29**, 1430011 (2014).
- [43] Planck Collaboration, N. Aghanim, Y. Akrami, M. Ashdown, J. Aumont, C. Baccigalupi, M. Ballardini, A. J. Banday, R. B. Barreiro, N. Bartolo *et al.*, *Astron. Astrophys.* **641**, A6 (2020).
- [44] A. Ringwald and C. Wetterich, *Nucl. Phys.* **B334**, 506 (1990).
- [45] J. Alexandre, V. Branchina, and J. Polonyi, *Phys. Lett. B* **445**, 351 (1999).
- [46] A. Bonanno and G. Lacagnina, *Nucl. Phys.* **B693**, 36 (2004).
- [47] J. Berges, N. Tetradis, and C. Wetterich, *Phys. Rep.* **363**, 223 (2002).
- [48] D. Benedetti and F. Caravelli, *J. High Energy Phys.* **06** (2012) 017; **10** (2012) 157(E).
- [49] M. Demmel, F. Saueressig, and O. Zanusso, *J. High Energy Phys.* **06** (2014) 026.
- [50] J. A. Dietz and T. R. Morris, *J. High Energy Phys.* **01** (2013) 108.
- [51] N. Ohta and M. Yamada, [arXiv:2110.08594](https://arxiv.org/abs/2110.08594).
- [52] G. Aliferis and V. Zariikas, *Phys. Rev. D* **103**, 023509 (2021).
- [53] A. B. Newman, T. Treu, R. S. Ellis, and D. J. Sand, *Astrophys. J.* **765**, 25 (2013).
- [54] A. Mitra and E. V. Linder, *Phys. Rev. D* **103**, 023524 (2021).
- [55] E. V. Linder and A. Mitra, *Phys. Rev. D* **100**, 043542 (2019).
- [56] A. G. Riess *et al.* (Supernova Search Team Collaboration), *Astron. J.* **116**, 1009 (1998).
- [57] S. Perlmutter *et al.* (Supernova Cosmology Project Collaboration), *Astrophys. J.* **517**, 565 (1999).
- [58] S. Alam *et al.* (eBOSS Collaboration), *Phys. Rev. D* **103**, 083533 (2021).
- [59] A. Fienga, J. Laskar, P. Exertier, H. Manche, and M. Gastineau, [arXiv:1409.4932](https://arxiv.org/abs/1409.4932).
- [60] F. Hofmann and J. Müller, *Classical Quantum Gravity* **35**, 035015 (2018).
- [61] E. P. Bellinger and J. Christensen-Dalsgaard, *Astrophys. J. Lett.* **887**, L1 (2019).
- [62] H. Yu, B. Ratra, and F.-Y. Wang, *Astrophys. J.* **856**, 3 (2018).
- [63] J. F. Jesus, R. Valentim, A. A. Escobal, and S. H. Pereira, *J. Cosmol. Astropart. Phys.* **04** (2020) 053.
- [64] P. Asimakis, S. Basilakos, N. E. Mavromatos, and E. N. Saridakis, *Phys. Rev. D* **105**, 083532 (2022).
- [65] E. N. Saridakis, W. Yang, S. Pan, F. K. Anagnostopoulos, and S. Basilakos, [arXiv:2112.08330](https://arxiv.org/abs/2112.08330).